PHOTONICS Research

Complex Swift Hohenberg equation dissipative soliton fiber laser

Ankita Khanolkar,[1] Yimin Zang,[1] and Andy Chong[1,2,*]

[1]Department of Electro-Optics and Photonics, University of Dayton, Dayton, Ohio 45469, USA
[2]Department of Physics, University of Dayton, Dayton, Ohio 45469, USA
*Corresponding author: achong1@udayton.edu

Received 12 January 2021; revised 28 March 2021; accepted 30 March 2021; posted 30 March 2021 (Doc. ID 419686); published 24 May 2021

Complex Swift Hohenberg equation (CSHE) has attracted intensive research interest over the years, as it enables realistic modeling of mode-locked lasers with saturable absorbers by adding a fourth-order term to the spectral response. Many researchers have reported a variety of numerical solutions of CSHE which reveal interesting pulse patterns and structures. In this work, we have demonstrated a CSHE dissipative soliton fiber laser experimentally using a unique spectral filter with a complicated transmission profile. The behavior and performance of the laser agree qualitatively with the numerical simulations based on CSHE. Our findings bring insight into dissipative soliton dynamics and make our mode-locked laser a powerful testbed for observing dissipative solitons of CSHE, which may open a new course in ultrafast fiber laser research.

https://doi.org/10.1364/PRJ.419686

1. INTRODUCTION

The cubic quintic Ginzberg Landau equation (CQGLE) can undoubtedly be used to describe a vast number of systems such as passively mode-locked lasers with fast saturable absorbers, parametric oscillators, wide aperture lasers, nonlinear optical transmission lines, and nonlinear cavities with the external pump [1–3]. In the CQGLE model, spectral filter transmission can be described by a quadratic term which leads to a Gaussian response. In the reality, the spectral filtering effect in mode-locked fiber lasers is a combination of gain spectrum and physical spectral filtering element inserted in the cavity, and the gain spectrum can exhibit non-uniform features. Therefore, to represent this condition, it is necessary to include higher-order terms while defining the profile of the spectral filter. The addition of a fourth-order spectral filtering term in the CQGLE model converts it into the complex Swift Hohenberg equation (CSHE).

The CSHE has played an important role in outlining pulse dynamics of various nonlinear optical systems such as large aspect lasers [4], photorefractive materials [5], semiconductor lasers [6], and passively mode-locked ultrafast lasers [7]. Despite the fact that some of the exact solutions of the CSHE can be obtained analytically [8], it seems that the CSHE can mainly be analyzed using numerical simulations [2,9,10]. Soto-Crespo *et al.* employed a fourth-order spectral filter in numerical simulations and found a great variety of soliton solutions such as composite pulses and moving solitons at anomalous dispersion [9]. In 2016, Latas reported numerical high energy soliton solutions of CSHE in both normal and anomalous dispersion regimes [11]. The energy of solitons generated in anomalous dispersion laser cavities is fundamentally limited according to the soliton area theorem [12,13]. The solution of CSHE at anomalous dispersion is dissipative solitons, which are less susceptible to the optical nonlinearities avoiding pulse breaking, and thus can have high energy compared to the solitons. Moreover, they possess linear chirp, which can be easily compensated to obtain ultrafast pulses. Therefore, the numerical result regarding high energy dissipative solitons at anomalous dispersion in Ref. [11] is particularly encouraging. Latas *et al.* also numerically analyzed erupting soliton solutions of CSHE by tuning the parameters of the spectral filter profile and higher-order effects [14]. In another noticeable effort, Zhao *et al.* numerically simulated an ytterbium (Yb) doped fiber laser cavity with a fourth-order spectral filter to obtain dissipative soliton resonance pulses [15].

Although extensive work has been already done numerically analyzing CSHE, very few efforts have been carried out for experimentally implementing a CSHE dissipative soliton fiber laser. Bao *et al.* were successful in observing switching dynamics of two dissipative soliton solutions of an erbium (Er) mode-locked fiber laser, and they discovered that the spectral filter with multiple transmission peaks was one of the critical parameters for the presence of this bistability [16]. Zhou *et al.* used composite filtering effect in an Er, Yb co-doped mode-locked fiber laser to observe mode-locked output to switch from a single soliton to a bound soliton state [17]. Both the papers focused more on the effect of a higher-order spectral filter on the pulse-switching dynamics, but they did not analyze the

mode-locked spectrum or pulse further to verify whether the laser output exhibited any similarity to the dissipative solitons of CSHE.

One of the obstacles in realizing a CSHE fiber laser is the unavailability of a commercial fourth-order spectral filter. In Ref. [17], three filters were combined to produce a composite filtering effect, and implementing such a complicated filter in a ring resonator is not feasible. Recently, we reported a birefringent fiber-based bandwidth tunable spectral filter which can generate a variety of transmission profiles [18]. This filter can control the value of the minimum in the spectral dip, the distance between the two maxima in the spectral response, as well as asymmetric maxima, which cannot be easily duplicated in a thin-film dielectric optical filter. In this paper, we have used the same fiber-based spectral filter along with a bandpass filter (BPF) to produce a higher-order spectral filter response which is then used in an Yb-doped fiber laser cavity that generates stable mode-locked pulses. These pulses are believed to be the moving soliton solutions of the CSHE as they depict asymmetric temporal profile as well as a highly asymmetric spectrum as predicted by Soto-Crespo *et al.* [9]. To the best of our knowledge, this is the first demonstration of a CSHE dissipative soliton fiber laser, and thus a first step in studying the effects of higher-order spectral filtering in mode-locked fiber lasers. We believe that our laser will provide an excellent platform to study the rich dynamics of dissipative solitons of CSHE.

2. EXPERIMENTAL SETUP

The experimental setup for the CSHE dissipative soliton fiber laser is sketched in Fig. 1. A wavelength division multiplexer (WDM) couples a 976 nm pump into 55 cm of Yb gain fiber followed by 1 m of single mode fiber (SMF). The mode locking relies on a saturable absorber, based on nonlinear polarization evolution, in the form of a polarization controller (PC1), half waveplate (HWP), quarter waveplate (QWP), and polarizing beam splitter (PBS). An isolator ensures the unidirectional operation of the laser. In order to create a fourth-order spectral filter transmission, a dual filter combination is used. The first filter is a birefringent fiber-based bandwidth tunable spectral filter (shown in Fig. 1). The lengths of the polarization-maintaining (PM) fibers in this filter are 10, 25, and 10 cm, respectively, and the length of SMF sections is 14.5 cm each. This spectral filter, combined with a 10 nm full width at half maximum (FWHM) BPF, gives a spectral response with two maxima. An 80/20 fused coupler is used to verify this spectral response. The total length of the fibers in the cavity is 5.54 m, and the total cavity dispersion is 0.127 ps^2.

3. NUMERICAL AND EXPERIMENTAL RESULTS

We performed numerical simulations for the laser configuration shown in Fig. 1 described by the CSHE:

$$A_z = -i\frac{\beta_2}{2}A_{tt} + \frac{\beta_3}{6}A_{ttt} + i\gamma_2|A|^2A + i\nu|A|^4A + \varepsilon|A|^2A + \mu|A|^4A + gA + (\delta A + \beta A_{tt} + \gamma A_{tttt}), \quad (1)$$

where $|A|$ is proportional to the electric field envelope of the pulse such that $|A|^2$ is its power, z is the propagation distance, and t is the retarded time. β_2 is the group velocity dispersion coefficient while β_3 is the third-order dispersion coefficient of the fiber. γ_2 represents the Kerr self-focusing nonlinearity and ν is the quintic nonlinearity, which is set to zero in this case. ε and μ are related to saturable absorption; g is the gain saturation, and is given by

$$g = \frac{g_0}{1 + \frac{E}{E_{sat}}}, \quad (2)$$

where E is the pulse energy given by

$$E = \int_{\frac{-T_R}{2}}^{\frac{T_R}{2}} |A|^2 dt, \quad (3)$$

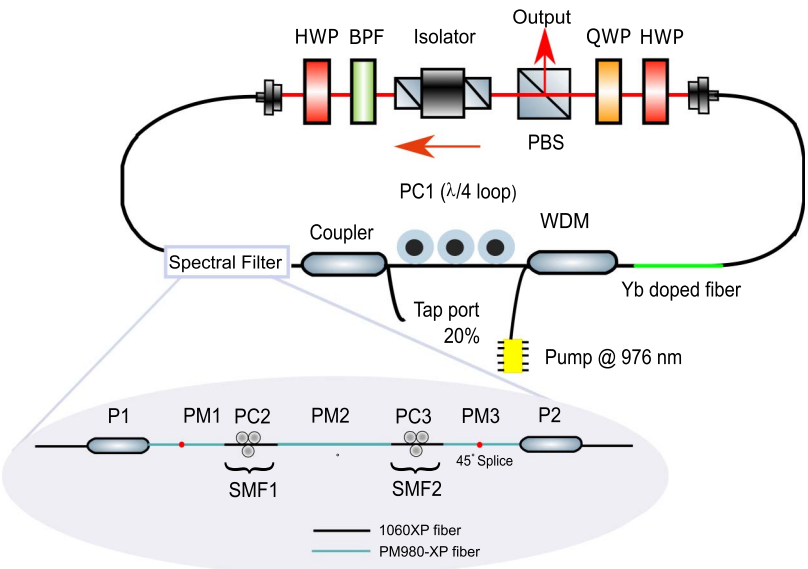

Fig. 1. Schematic of the fiber oscillator. PBS, polarizing beam splitter; HWP, half waveplate; QWP, quarter waveplate; BPF, bandpass filter; PC, polarization controller; WDM, wavelength division multiplexer; P, in-line polarizer; PM, polarization-maintaining; SMF, single mode fiber.

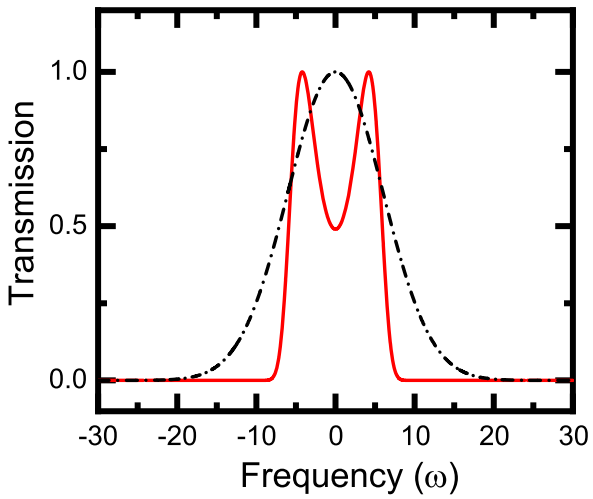

Fig. 2. Spectral filter transmission $T(\omega) = e^{\delta-\beta\omega^2-\gamma\omega^4}$ in the CQGLE model (dashed curve) with $\delta = 0$, $\beta = 0.012$, and $\gamma = 0$ and the CSHE model (solid curve) with $\delta = -0.7133$, $\beta = -0.0809$, and $\gamma = 0.0023$.

where T_R is the cavity roundtrip time, E_{sat} is the saturation energy, and g_0 is the small signal gain. The terms containing δ, β, and γ describe the spectral response, the transmission of which is given by

$$T(\omega) = e^{\delta-\beta\omega^2+\gamma\omega^4}. \tag{4}$$

The main difference between the CSHE and the CQGLE lies in the fourth-order spectral filtering term with γ. With γ set to zero and with a positive β, a single peak spectral filter can be obtained, whereas a positive γ and a negative β yield a spectral response with two maxima. Figure 2 shows the parameters of the spectral filter used in the simulation along with the spectral filter in the CQGLE model, with the same bandwidth as the former one.

We assume the initial pulse shape to be hyperbolic secant for our simulations. The fiber parameters considered for the simulation roughly follow the experimental condition and are $\gamma_2 = 0.0047\ \text{W}^{-1}\text{m}^{-1}$ for SMFs and YDFs, and $\beta_2 = 23\ \text{fs}^2/\text{mm}$ and $\beta_3 = 63.8\ \text{fs}^2/\text{mm}$ for SMFs and YDFs, respectively. It should be noted that β_3 is considered in this simulation to trigger the asymmetric pulse generation. In the absence of β_3, the initial symmetric pulse does not evolve into an asymmetric pulse. Alternatively, one can simulate CSHE without the third-order dispersion term but using an initial simulation condition similar to Ref. [9], i.e., hyperbolic secant pulse profile with an asymmetric phase (i.e., a pulse with an initial velocity) which will result in an asymmetric output pulse. We prefer β_3 to be the asymmetry trigger over the initial pulse with asymmetric phase, as it is a better match to the experimental conditions. The other simulation parameters are g_0, which corresponds to 30 dB of small signal gain, and $E_{\text{sat}} = 900$ pJ. The output coupler has a 70:30 coupling ratio. The saturable absorber used in the simulation is a monotonic saturable absorber with the transmittance $T = 1 - q_0/[1 + P(t)/P_{\text{sat}}]$, where $q_0 = 1$ is the modulation depth, $P(t)$ is the instantaneous pulse power, and $P_{\text{sat}} = 0.7$ kW is the saturation power. The corresponding ε and μ parameters are $5.19 \times 10^{-4}\ \text{W}^{-1}\,\text{m}^{-1}$ and $-7.42 \times 10^{-7}\ \text{W}^{-2}\,\text{m}^{-1}$, respectively. Figure 3(a) shows the result of propagating the initial pulse profile over the number of roundtrips (N), which quickly

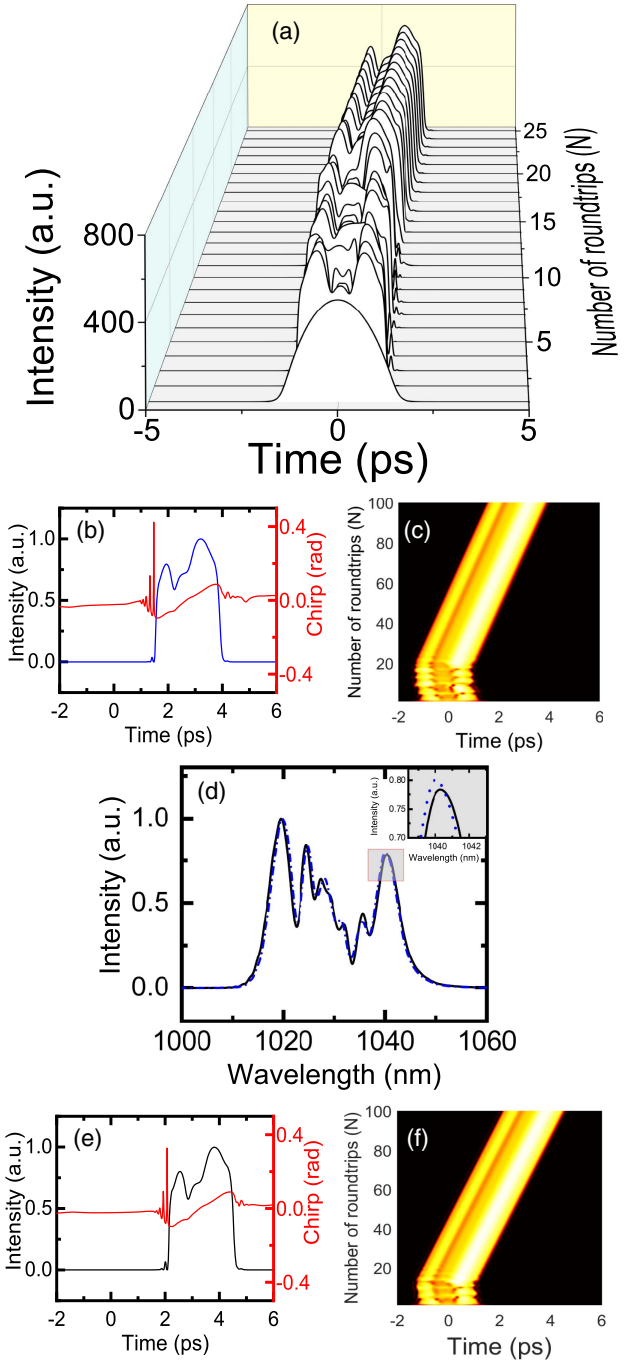

Fig. 3. Numerical simulation results. (a) Pulse evolution in the presence of the spectral filter. (b) Asymmetric pulse profile (blue curve) along with its chirp (red curve). (c) Amplitude contour plot explaining temporal dynamics of the moving pulse. (d) Asymmetric mode-locked spectrum (dashed blue curve) pertaining to the moving pulse solution in (c) and more asymmetric mode-locked spectrum (solid black curve) related to different simulation parameters. The inset shows the asymmetry at the longer wavelength tail of the spectra. (e) Pulse profile and the chirp associated with the more asymmetric mode-locked spectrum. (f) Temporal dynamics of the moving pulse solution related to the more asymmetric mode-locked spectrum.

converges to a pulse profile that is asymmetric in shape with unequal shoulders [blue curve in Fig. 3(b)]. The output pulses are chirped and the red curve in Fig. 3(b) depicts the chirp across the central region of the pulse. Interestingly, this is a moving pulse solution and the pulses are moving faster, as illustrated in Fig. 3(c). This behavior quite closely matches with the moving pulse solution depicted by Ref. [9]. The dashed blue curve in Fig. 3(d) shows that the spectrum of these pulses is also asymmetric, featuring two unequal maxima. By slightly changing the saturable energy of the gain fiber and saturation power of the saturable absorber, it is possible to get a slightly different and more asymmetric spectrum [shown by the solid black curve in Fig. 3(d)]. It should be noted that the pulses associated with this spectrum [shown in Fig. 3(e)] are moving a little slower (more negative velocity) than the case shown in Fig. 3(c), which is presented in Fig. 3(f). This agrees with the observation in Ref. [9] that the greater the asymmetry of the spectrum, the higher the velocity of moving pulses irrespective of the sign of the velocity.

One may think that the β_3 is the cause of temporal and spectral asymmetry in the CSHE simulation results presented in Fig. 3. On the contrary, the fourth-order spectral filter is the main reason for the output pulse and spectrum to be asymmetric. It has already been studied that including β_3 in the CQGLE simulation has very little to no influence on the output pulse [19]. This proves that a filter with Gaussian response is incapable of generating an asymmetric moving pulse solution even if the β_3 is taken into account, and therefore the asymmetric moving soliton solution can be tied to the fourth-order spectral filter.

Initially, the laser cavity is operated below the lasing threshold at a pump power of 50 mW to observe the transmission profile of the spectral filter by coupling amplified spontaneous emission (ASE) (shown by a dashed curve in Fig. 4) into the spectral filter and observing the filter output through the 20% port of the fiber coupler. The PC2 and PC3 are carefully tuned so that the output of the spectral filter exhibits a multiple peak structure with a dip at 1030 nm (dotted curve in Fig. 4).

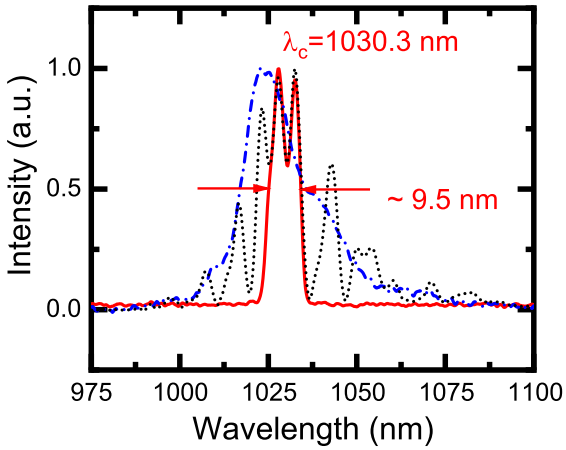

Fig. 4. Output of the fiber-based filter and BPF combination (solid curve) with ASE (dashed line) as input. The dotted line depicts the output of fiber-based filter only.

Although this spectral filter transmission shows multiple peaks around 1030 nm, the laser fails to mode-lock using such a filter. It could be attributed to the two factors: the wide bandwidth of the filter transmission and the presence of unwanted sinusoidal structure in the filter transmission. To mitigate this problem, a BPF with 10 nm FWHM bandwidth is introduced in the cavity to select a double-peak transmission out of the multi-peak structure, and the resulting shape of the spectral filter is presented by the solid curve in Fig. 4. The same spectral filter response is used in all the experiments discussed in this work.

The initial mode-locking is obtained by rotating intracavity waveplates and by adjusting PC1 at a pump power of ~400 mW. But this initial mode-locked spectrum is not very stable for the long duration of the experiments, and hence the pump power is increased. A stable mode-locking is achieved at 545 mW of input pump power; the output spectrum ejected by the PBS is recorded and shown in Fig. 5(a) and, as predicted by simulation, it is asymmetric and much wider than the spectral filter. The spectrum transmitted through the PBS is filtered out by the localized spectral filter; this filtered spectrum can be observed through the 20% port of the fiber coupler and is displayed in Fig. 5(b), and it proves that the spectrum circulating the laser cavity always remains asymmetric. The output pulse profile is measured performing a cross-correlation between the chirped pulse directly emitted from the laser and the de-chirped pulse obtained from a grating pair compressor, and is presented

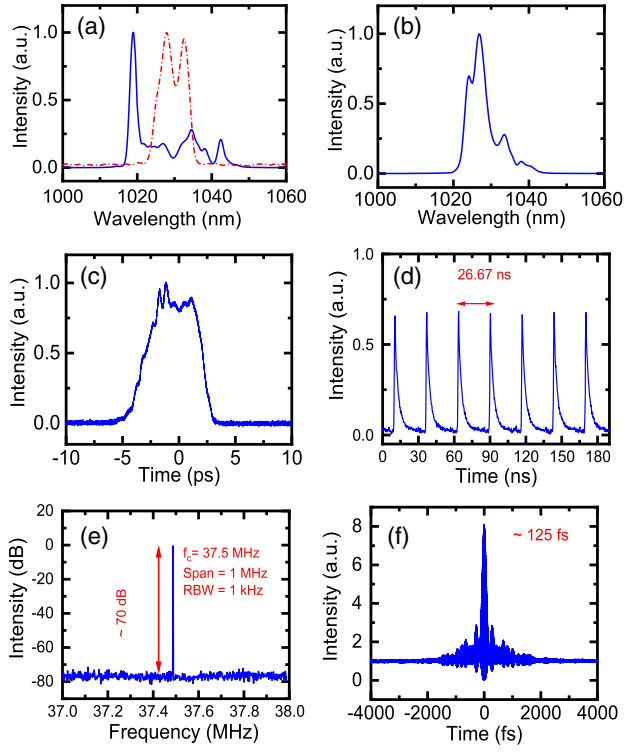

Fig. 5. Experimental dataset recorded at 545 mW of input pump power. (a) Mode-locked spectrum at the PBS (solid curve) along with the spectral filter response (dashed curve). (b) Spectrum obtained at the 20% port of the fiber coupler. (c) Cross-correlation of the output pulse. (d) Pulse train. (e) RF spectrum. (f) Autocorrelation.

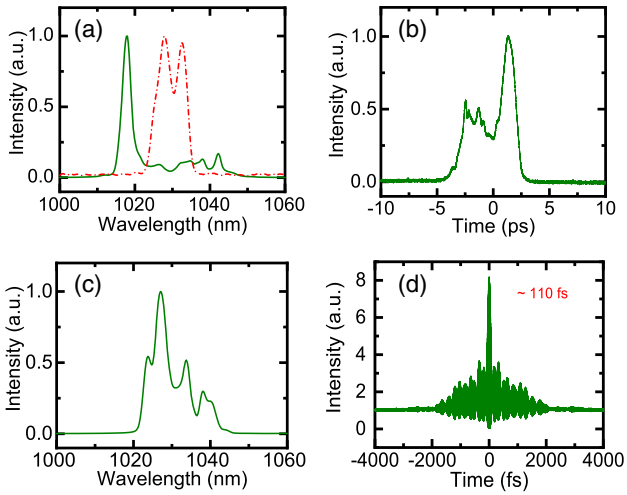

Fig. 6. Experimental dataset recorded at 571 mW of input pump power. (a) Mode-locked spectrum with a spectral filter response (dashed curve). (b) Cross-correlation of the output pulse. (c) Spectrum obtained at the 20% port of the fiber coupler. (d) Autocorrelation.

in Fig. 5(c). It matches with the numerical simulation in terms of the asymmetric structure with the unequal shoulders. The laser produces a stable pulse train [Fig. 5(d)] with ~37.5 MHz repetition rate. The average mode-locked output power is 75 mW, which corresponds to a pulse energy of ~2 nJ. Figure 5(e) depicts a radio frequency (RF) spectrum measured with a high-resolution RF spectrum analyzer (Agilent N9914A). There are no residual sidebands at least 70 dB below the carrier. Also, stable single pulsing is verified with a ns photodiode and by monitoring the interferometric autocorrelation. The de-chirped pulse duration is ~125 fs [Fig. 5(f)]. Another mode-locked spectrum is obtained by slightly changing the orientation of the HWP from the saturable absorber and at an increased pump power. This slightly broad mode-locked spectrum is illustrated in Fig. 6(a) at the maximum pump power of 571 mW. It is important to note that the spectrum and pulse [Fig. 6(b)] still retain their asymmetric profiles. Figure 6(c) displays the spectrum at the 20% port of the coupler. The interferometric autocorrelation in Fig. 6(d) shows that the pulse width has narrowed down a little to ~110 fs. The average mode-locked output power is 105 mW which corresponds to a pulse energy of ~2.8 nJ.

Figure 7(a) offers insight into the asymmetry between the two mode-locked spectra. Spectrum 1 is less asymmetric than spectrum 2, and therefore it is expected that the solitons associated with spectrum 1 will move slightly faster than the ones associated with spectrum 2. This is verified by observing change in the repetition rate of the laser. A short span of 1 kHz and a high resolution bandwidth of 1 Hz are used to record the RF spectra for these two modes, and the results are shown in Fig. 7(b). The repetition rate corresponding to the mode-locked spectrum 1 is higher by ~100 Hz than that of spectrum 2. This matches with our theoretical prediction that the higher asymmetric spectrum travels slower, which results in the reduced repetition rate of the laser.

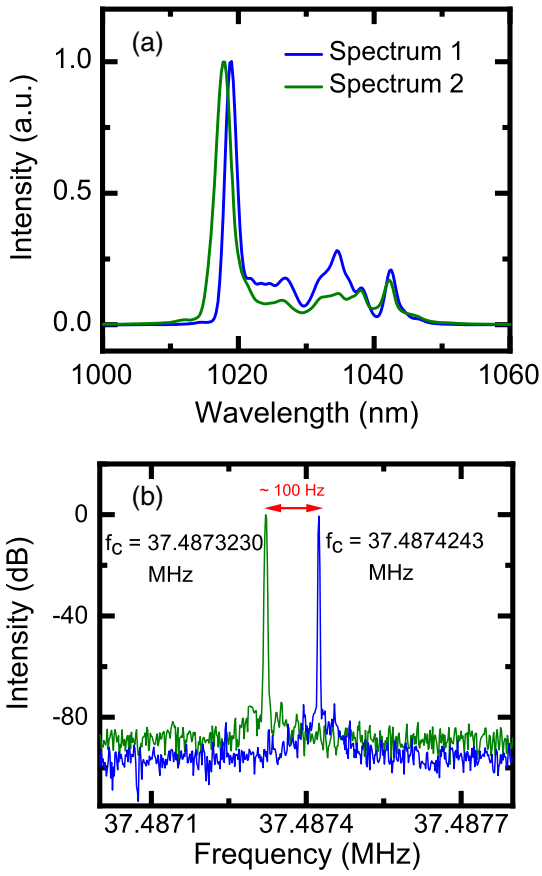

Fig. 7. Comparison between the two experimental datasets. (a) Asymmetry comparison between the two mode-locking states. The blue curve (spectrum 1) depicts the spectrum for the mode at 545 mW input pump power while the green curve (spectrum 2) denotes the spectrum for the mode measured at 571 mW. (b) Repetition rate comparison between the two spectra.

4. DISCUSSION

Our simulation and experimental results can be a starting point to explore this pulse-shaping mechanism based on the fourth-order spectral filtering in the mode-locked fiber lasers. We were successful in realizing dissipative solitons of CSHE fiber lasers with a strong indication of the moving pulse solution of CSHE, characterized by an asymmetric pulse profile with an asymmetric spectrum. In this paper, for the numerical simulations as well as the experiment, we have considered only one spectral filter response, defined by specific values of δ, β, and γ. However, the prospects of finding other solutions of the CSHE in mode-locked fiber lasers using different spectral filter responses are very promising. In the experiments, an all-fiber-based spectral filter along with the BPF is perfectly capable of producing a spectral filter transmission not only of the fourth order but also higher orders. Studying the effects of such a higher-order spectral filter in mode-locked fiber lasers will be interesting.

It is well known that pulse energy is one of the most important performance parameters of the ultrafast fiber lasers. In our experiments, the pulse energy can reach up to 3 nJ but

is limited by the input pump power. We believe that the pulse energy can be improved significantly by realizing the same laser cavity using double-clad fibers. It has already been proven numerically that CSHE can have high energy solutions at both normal and anomalous dispersion [11]. For the mode-locked lasers at anomalous dispersion, the generated conventional solitons have limited applications due to low pulse energies. Therefore, there is an increasing interest in researching whether high performance dissipative solitons can be experimentally obtained in anomalous dispersion regime [20,21], and realizing CSHE fiber laser at anomalous dispersion may be a possible way to achieve this goal.

5. CONCLUSION

In conclusion, we report the first observation, to our knowledge, of dissipative solitons of CSHE in a passively mode-locked fiber laser. A dual filter in the form of unique fiber-based filter along with a BPF easily produces a fourth-order spectral response. The generated pulses have complex asymmetric profiles and the laser spectrum is highly asymmetric, with the pulse energy approaching 3 nJ and pulse duration of ~100 fs. Much work still remains to optimize the performance of this laser, but we believe that our studies provide the basis for further investigation of pulse dynamics in mode-locked fiber laser systems with higher-order spectral filtering.

Funding. National Science Foundation (EECS 1710914).

Acknowledgment. The authors thank Monish Chatterjee and Julie Motz for providing the RF spectrum analyzer. The authors also thank Imad Agha for lending a polarization controller for the experiments.

Disclosures. The authors declare no conflicts of interest.

REFERENCES

1. H. A. Haus, "Theory of mode locking with a fast saturable absorber," J. Appl. Phys. **46**, 3049–3058 (1975).
2. N. Akhmediev and A. Ankiewicz, *Dissipative Solitons: From Optics to Biology and Medicine* (Springer, 2008), Vol. **751**.
3. W. Firth and A. Scroggie, "Optical bullet holes: robust controllable localized states of a nonlinear cavity," Phys. Rev. Lett. **76**, 1623–1626 (1996).
4. J. Lega, J. V. Moloney, and A. C. Newell, "Swift–Hohenberg equation for lasers," Phys. Rev. Lett. **73**, 2978–2981 (1994).
5. K. Staliūnas, G. Šlekys, and C. Weiss, "Nonlinear pattern formation in active optical systems: shocks, domains of tilted waves, and cross-roll patterns," Phys. Rev. Lett. **79**, 2658–2661 (1997).
6. J.-F. Mercier and J. V. Moloney, "Derivation of semiconductor laser mean-field and Swift–Hohenberg equations," Phys. Rev. E **66**, 036221 (2002).
7. E. P. Ippen, "Principles of passive mode locking," Appl. Phys. B **58**, 159–170 (1994).
8. K.-I. Maruno, A. Ankiewicz, and N. Akhmediev, "Exact soliton solutions of the one-dimensional complex Swift–Hohenberg equation," Phys. D **176**, 44–66 (2003).
9. J. M. Soto-Crespo and N. Akhmediev, "Composite solitons and two-pulse generation in passively mode-locked lasers modeled by the complex quintic Swift–Hohenberg equation," Phys. Rev. E **66**, 066610 (2002).
10. H. Wang and L. Yanti, "An efficient numerical method for the quintic complex Swift-Hohenberg equation," Numer. Math. Theory Methods Appl. **4**, 237–254 (2011).
11. S. Latas, "High-energy plain and composite pulses in a laser modeled by the complex Swift–Hohenberg equation," Photon. Res. **4**, 49–52 (2016).
12. H. Haus, E. Ippen, and K. Tamura, "Additive-pulse modelocking in fiber lasers," IEEE J. Quantum Electron. **30**, 200–208 (1994).
13. L. E. Nelson, D. Jones, K. Tamura, H. Haus, and E. Ippen, "Ultrashort-pulse fiber ring lasers," Appl. Phys. B **65**, 277–294 (1997).
14. S. Latas, M. Ferreira, and M. Facão, "Swift–Hohenberg soliton explosions," J. Opt. Soc. Am. B **35**, 2266–2271 (2018).
15. L. Zhao, D. Li, L. Li, X. Wang, Y. Geng, D. Shen, and L. Su, "Route to larger pulse energy in ultrafast fiber lasers," IEEE J. Sel. Top. Quantum Electron. **24**, 8800409 (2017).
16. C. Bao, W. Chang, C. Yang, N. Akhmediev, and S. T. Cundiff, "Observation of coexisting dissipative solitons in a mode-locked fiber laser," Phys. Rev. Lett. **115**, 253903 (2015).
17. Y. Zhou, W. Lin, H. Cheng, W. Wang, T. Qiao, Q. Qian, S. Xu, and Z. Yang, "Composite filtering effect in a SESAM mode-locked fiber laser with a 3.2-Ghz fundamental repetition rate: switchable states from single soliton to pulse bunch," Opt. Express **26**, 10842–10857 (2018).
18. A. Khanolkar, X. Ge, and A. Chong, "All-normal dispersion fiber laser with a bandwidth tunable fiber-based spectral filter," Opt. Lett. **45**, 4555–4558 (2020).
19. A. Chong, W. H. Renninger, and F. W. Wise, "Route to the minimum pulse duration in normal-dispersion fiber lasers," Opt. Lett. **33**, 2638–2640 (2008).
20. X. Wang, Y.-G. Liu, Z. Wang, Z. Wang, and G. Yang, "L-band efficient dissipative soliton erbium-doped fiber laser with a pulse energy of 6.15 nJ and 3 dB bandwidth of 47.8 nm," J. Lightwave Technol. **37**, 1168–1173 (2019).
21. J. Zhou, W. Qi, W. Pan, and Y. Feng, "Dissipative soliton generation from a large anomalous dispersion ytterbium-doped fiber laser," Opt. Lett. **45**, 5768–5771 (2020).